VIP Biocatalysis Very Important Paper

International Edition: DOI: 10.1002/anie.201501778
German Edition: DOI: 10.1002/ange.201501778

How the [$NiFe_4S_4$] Cluster of CO Dehydrogenase Activates CO_2 and NCO^-**

*Jochen Fesseler, Jae-Hun Jeoung, and Holger Dobbek**

Abstract: *Ni,Fe-containing CO dehydrogenases (CODHs) use a [$NiFe_4S_4$] cluster, termed cluster C, to reversibly reduce CO_2 to CO with high turnover number. Binding to Ni and Fe activates CO_2, but current crystal structures have insufficient resolution to analyze the geometry of bound CO_2 and reveal the extent and nature of its activation. The crystal structures of CODH in complex with CO_2 and the isoelectronic inhibitor NCO^- are reported at true atomic resolution ($d_{min} \leq 1.1$ Å). Like CO_2, NCO^- is a μ_2,η^2 ligand of the cluster and acts as a mechanism-based inhibitor. While bound CO_2 has the geometry of a carboxylate group, NCO^- is transformed into a carbamoyl group, thus indicating that both molecules undergo a formal two-electron reduction after binding and are stabilized by substantial π backbonding. The structures reveal the combination of stable μ_2,η^2 coordination by Ni and Fe2 with reductive activation as the basis for both the turnover of CO_2 and inhibition by NCO^-.*

The efficient reduction of carbon dioxide (CO_2) into added-value products is of great economical and ecological importance.[1] The crucial step in these multielectron, multiproton processes is the initial activation of CO_2 and its subsequent splitting into CO and water ($CO_2 + 2e^- + 2H^+ \rightarrow CO + H_2O$).[2] Owing to the thermodynamic stability and kinetic inertness of CO_2, heterogeneous catalysis by metals on electrode surfaces or homogenous catalysis by transition-metal complexes is required for turnover under ambient temperatures and pressures.[3] However, commercial catalysts are typically instable, have low turnover rates, and need to be operated under high overpotentials. Several anaerobic bacteria and archaea employ Ni,Fe-containing CO dehydrogenases (CODHs) as catalyst for rapid and efficient CO_2/CO transformation.[3c,4] CODHs catalyze CO_2 reduction with rates of 12 s^{-1} and CO oxidation with rates of up to 40000 s^{-1}.[5] Their active sites harbor a [$NiFe_4S_4$–OH_x] cluster (cluster C),[4a,6] which cycles between at least two catalytically relevant oxidation states: C_{red2} is competent for CO_2 reduction and C_{red1} for CO oxidation. The two states differ by two electrons and have an operational midpoint potential of −530 mV, which coincides with the values found for the CO_2/CO pair ($E^{\circ\prime} = -558$ mV).[7] Crystallographic studies of a cryo-trapped CO_2-bound state generated under turnover conditions revealed a CO_2 ligand bridged between Ni and Fe2 in a μ_2,η^2 coordination geometry as key intermediate in the catalysis.[6] However, the limited resolution of 1.5 Å prevented a detailed analysis of the bond lengths and angles of the bound CO_2, the geometry of which had to be restrained for refinement and was thus lacking the information needed to analyze bond order, degree of activation, and geometric strain in the ligands.

The purpose of this study was to resolve how CO_2 is bound and activated at cluster C. Since CO_2 is turned over under the chosen conditions and may thus exist in different superimposing states in the structure, we also investigated binding of the inhibitor NCO^- as a reference point for our analysis. Cyanate (NCO^-) is isoelectronic and isostructural to CO_2 and selectively inhibits CO_2 reduction in the C_{red2} state, while CO oxidation is virtually unaffected.[8] We determined the structures of CODH II of *Carboxydothermus hydrogenoformans* (CODH-II_{Ch}) under reducing conditions ($E^{\circ\prime} = -600$ mV) at true atomic resolution in the presence of HCO_3^-/CO_2 ($d_{min} = 1.03$ Å) and NCO^- ($d_{min} = 1.09$ Å). The resolution allowed refinement of the structures without stereochemical restraints and individual atomic positions are defined, including estimates for standard deviations for the bond lengths and bond angles. The CO_2-bound state appears fully accumulated with a Ni/CO_2 ratio of 1:1 as judged by refinement statistics (Table S1 in the Supporting Information). Electron density maps clearly revealed a triatomic ligand bound to Ni and Fe2 (also known as ferrous-component II, FCII) of cluster C and were consistent with bent CO_2 (Figure 1a). In the presence of NCO^-, a bridging ligand with a μ_2,η^2 coordination similar to CO_2 was observed connecting Ni and Fe2. The ligand was modeled as NCO^-, refining to a Ni/NCO^- ratio of 1:1, thus indicating full accumulation in the crystal (Figure 1b).

The true atomic resolution allowed us to attribute individual atomic positions and differences in electron numbers, for example, electron densities are significantly stronger for oxygen atoms compared to the central carbon atom of the ligand (Figure 1a). The cluster-bound CO_2 has an occupancy of 57%, which is identical to the refined occupancy of Ni (57%). Interactions of CO_2 with the protein matrix are mainly due to hydrogen bonds to His93 and Lys563, with distances of 2.72 and 2.70 Å, respectively.

[*] J. Fesseler, Dr. J.-H. Jeoung, Prof. Dr. H. Dobbek
Institut für Biologie, Strukturbiologie/Biochemie
Humboldt-Universität zu Berlin
Unter den Linden 6, 10099 Berlin (Germany)
E-mail: holger.dobbek@hu-berlin.de

[**] We thank the German Research Foundation for funding through project grant DO-785/5-1 and the Cluster of Excellence "Unifying Concepts in Catalysis—UniCat" (EXC 314). Rainer Dietrich and Silke Steinborn are acknowledged for excellent technical assistance. We thank Dr. Tobias Werther for help with geometric analysis. We further acknowledge access to Beamlines of the BESSY II storage ring (Berlin (Germany)) via the Joint Berlin MX-Laboratory at the Helmholtz Zentrum Berlin.

Supporting information for this article is available on the WWW under http://dx.doi.org/10.1002/anie.201501778.

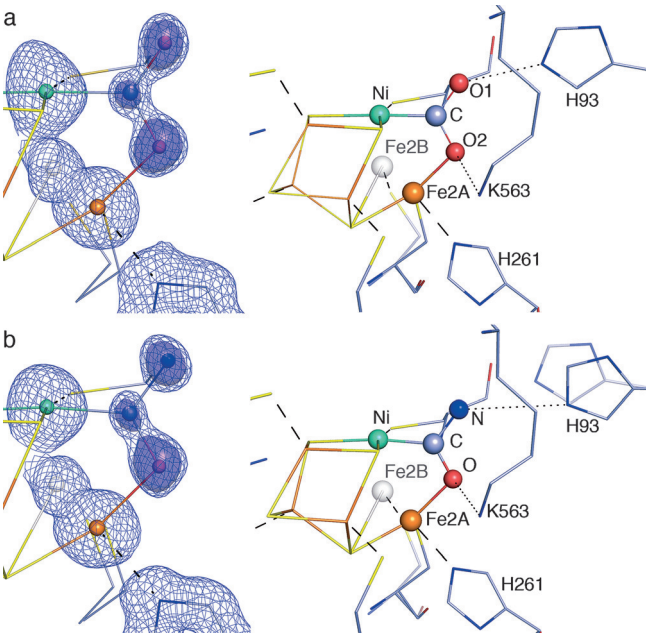

Figure 1. Structures of CO_2 and NCO^- bound to cluster C at true atomic resolution. a) Cluster C with CO_2 (d_{min}: 1.03 Å). b) Cluster C with NCO^- (d_{min}: 1.09 Å). $2F_o-F_c$ maps (blue mesh, contour level: 1.75 σ and purple isosurface contoured at 2.5 σ) are shown together with the refined model. The panels on the right shows ball-and-stick models of cluster C and the second coordination sphere. C Gray-blue, N blue, O red, S yellow, Fe orange, and Ni cyan.

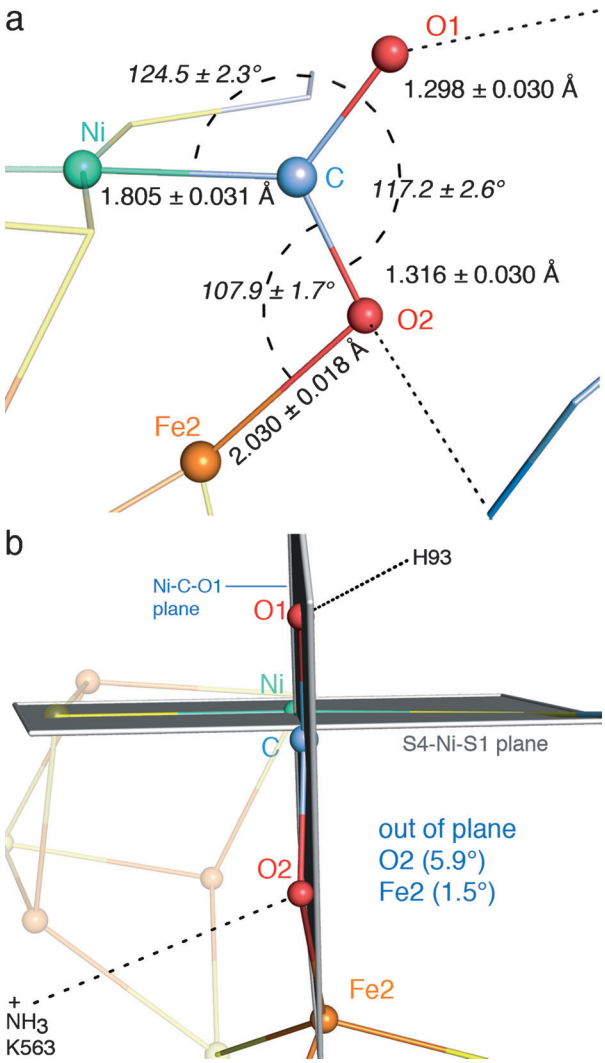

Figure 2. Geometry analysis of CO_2 bound to cluster C. a) Individual bond distances and angles with their standard deviations estimated by inversion of the least-squares matrix. b) Plane distortion analysis. The Ni–C axis points towards the reader. The S4-Ni-S1 and Ni-C-O1 planes are shown in black. CO_2 bound to cluster C is shown as a ball-and-stick model. Ni, C, N, O, and Fe are highlighted as spheres and colored as in Figure 1.

Activation of small molecules like CO_2 or NCO^- is achieved through a reduction in bond energy and order and manifests in elongated bonds and distortions from linearity. To derive a least-biased geometry for both ligands, including standard deviations for their bond lengths and bond angles, we employed an inversion of the full least-squares correlation matrix without the inclusion of geometrical restraints after a conclusive refinement using SHELXL-2014.[9] The results of the analysis are summarized in Figure 2 for CO_2-bound cluster C and Figure 3 for NCO^--bound cluster C.

CO_2 bound to cluster C differs from free CO_2, which is linear and has bond lengths of 1.16 Å.[10] The C–O1 and C–O2 bonds are substantially elongated in the bound CO_2 and with bond lengths of 1.30 and 1.32 Å are almost identical in length (Figure 2), which is unexpected. First, in μ_2-η^2 complexes, CO_2 typically has one shorter and one longer C–O bond, where the longer bond is connected to the bridged second metal.[11] Second, as one C–O bond in CO_2 is cleaved during the reaction, "priming" of the scissile C–O bond through stretching of the bond is expected.

The major advance of true atomic resolution data became evident when we compared the new structure with the structure of the CO_2-bound state as determined at 1.5 Å resolution.[6] The structures differ substantially in the position of the carbon atom of bound CO_2 (see Figure S1 in the Supporting Information). The resulting Ni–C bond is substantially shorter than determined earlier and at 1.81 Å is among the shortest Ni–C bonds reported.

The change in position of the carbon atom of CO_2 is also responsible for the large change in the O-C-O angle. Activation of CO_2 by electronic excitation, formation of a radical anion species ($CO_2^{\bullet-}$), or adduct formation with an electron-rich species will populate the lowest unoccupied molecular orbital (LUMO) and result in a distortion from linearity.[12] A bent geometry with an O-C-O angle close to 133° has been frequently observed and reflects a value for which electron repulsion and molecular energy are minimized.[13] The structure of Ni,Fe-CODH with bound CO_2 at a resolution of 1.5 Å reported earlier was in agreement with an O-C-O angle of about 130°, thus formally the anionic radical $CO_2^{\bullet-}$.[6] Remarkably the O-C-O angle is 15° smaller than estimated earlier, thus indicating a higher degree of reductive CO_2 activation. The angle of 117° observed in the true atomic resolution structure is similar to that found in formate (123°) and is also comparable to the geometry found for η^1-coordinated carboxylate at mononuclear Ni centers

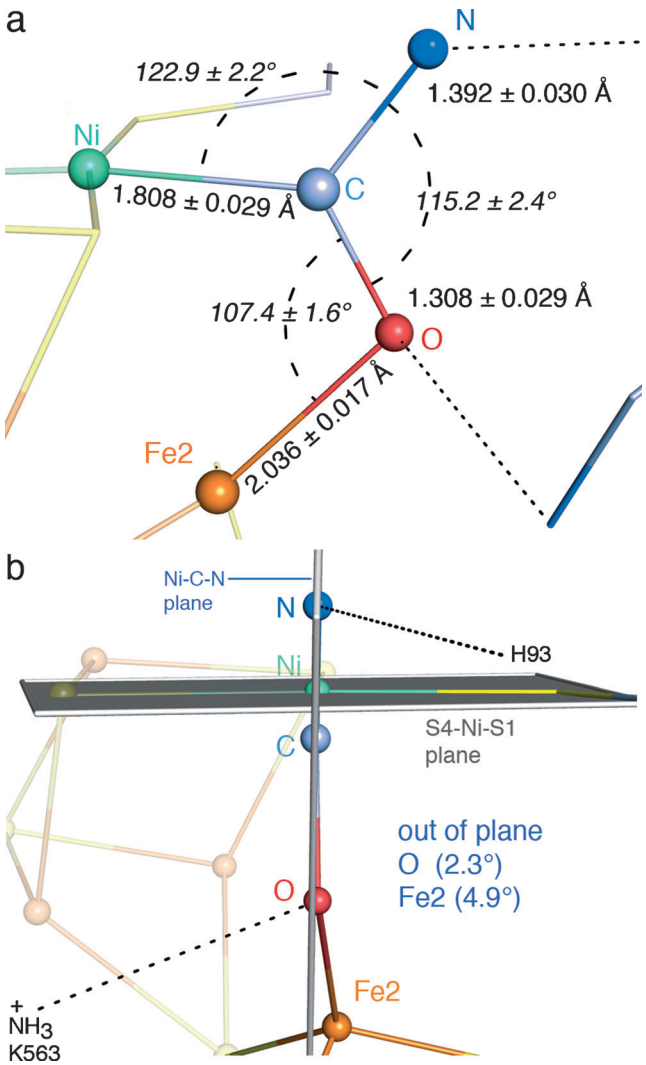

Figure 3. Geometry analysis of NCO^- bound to cluster C. a) Individual bond distances and angles with their standard deviations estimated by inversion of the least-squares matrix. b) Plane distortion analysis. The Ni–C axis points towards the reader. The S4-Ni-S1 and Ni-C-O1 planes are shown in black. NCO^- bound to cluster C is shown as a ball-and-stick model. Ni, C, N, O, and Fe are highlighted as spheres and colored as in Figure 1.

(119.6°) or μ_2,η^2-coordinated bimetallic complexes with Re,Re (119.0°) or Re,Sn (117.0°) centers.[14]

To gain further insight into the nature of the ligands, DFT calculations (Jaguar 8.6, B3LYP, LACV3P**) were conducted for the ligand structures found in the active site. We first analyzed the dependency of the C–N/O bond length and N/O-C-O angle on the charge of the fragments. The crystallographically observed bond lengths and angles best match CO_2^{2-} and H_2NCO^- fragments, with the largest deviations between observed and calculated values of 0.05 Å for the bond lengths and 3° for the bond angles. Natural bond orbital analysis indicated that the two additional electrons of CO_2^{2-} increase the charge at the carbon atom by nearly one electron and increase the charge of each oxygen atom by approximately 0.5 electrons. The natural Lewis structure is strongly delocalized and the electron lone pairs centered at the p molecular orbital (MO) of the oxygen atoms act as donors to the π* MOs of the other C–O bond. In contrast to CO_2, where the electron lone pairs are only found at the oxygen atoms, CO_2^{2-} has a carbon-centered lone pair with $sp^{0.74}$ character. The short Ni–C bond indicates substantial π backbonding in the Ni–CO_2 complex, in which CO_2^{2-} may act as a σ donor (formal electron lone pair at C in the fragment) and π acceptor (π* MO centered at C) with the $3d_{xy}$ orbital at Ni as a possible π donor MO. The π backdonation of electrons is equivalent to a metal-to-ligand charge transfer and increases the flux of electrons from the metal to the ligand.

The Ni ion of cluster C lies at the intersection of two planes: a horizontal plane defined by S4-Ni-S1 and a vertical plane nearly perpendicular (92.2°) to it (Figure 2b). With substrate bound to cluster C, the atoms Ni-C-O1 may define the vertical plane for CO_2. The carbon atom is only 0.09 Å below the S4-Ni-S1 plane and cluster C achieves an almost ideal square-planar arrangement around Ni despite tight spatial constraints. A slight distortion of O2 from the Ni-C-O1 plane is evident in the bound CO_2 (Figure 2b). The resulting distance of 0.119 Å and angular deviation of 5.9° of O2 from the plane indicate that the CO_2 molecule no longer lies perfectly within the plane. The distortion of the Fe-bound O2 of CO_2 from the plane shifts it in the direction of the amino group of Lys563, a residue important for catalysis.[15] However, this small distortion is unlikely to contribute significantly to the catalytic reduction of CO_2.

Overall, the geometry of bound CO_2 suggests that following bifunctional attack of a nucleophilic Ni center and an electrophilic Fe center, a flow of electrons from the cluster to CO_2 occurs, thereby rendering the ligand more similar to the two-electron-reduced carboxylate group than to CO_2. To investigate whether the reductive bifunctional attack is also responsible for the oxidation-state-specific inhibition of CODH by NCO^- and to compare CO_2 and NCO^- binding, we resolved the CODH–NCO^- structure at atomic resolution. The NCO^--bound state is remarkably similar to the CO_2-bound state, with nearly identical bond angles and similar bond lengths, including the short Ni–C bond (Figure 3).

NCO^- is an ambidentate ligand and O-bonded as well as N-bonded NCO^- complexes are found.[16] NCO^- appears as a linear ligand in monometallic complexes and in the rare bimetallic complexes, where it bridges two metals.[17] The bent geometry of NCO^- observed in this study is atypical and further underpins the unique reactivity of cluster C.

Bond lengths and angles encountered for the NCO^--moiety agree well with the values calculated for a carbamoyl fragment, from which only the C–NH_2 bond length deviates slightly (r_{C-N} = 1.44 Å in the model, 1.39 Å in this study). The N, C, and O atoms of the ligand are nearly perfectly aligned together with Ni and Fe2 in one plane (Figure 3b) and the Ni-C-N plane is, as in the case of bound CO_2, perpendicular to the S4-Ni-S1 plane (angle between both planes: 88.8°). Compared to bound CO_2 the N-C-O plane is tilted 1.8° (see Figure S2).

The proposed two-electron reduction of bound NCO^- to a carbamoyl group is also supported by a conformational change in the active site. The binding of NCO^- to cluster C changes the conformation of His93, which is shifted by 1.36 Å

compared to the position found in free and CO_2-bound CODH, thereby increasing the distance between the N of NCO^- and the Nε atom of His93 to 3.63 Å. In a second conformation with lower occupancy (35%), His93 is in the same position as in CO_2-bound and free CODH and this conformation corresponds to the fraction of active sites without NCO^- bound. The likely driving force for the conformational change of His93 is the space required for the two hydrogen atoms of the carbamoyl group and the associated switch from a hydrogen-bond acceptor function to a hydrogen-bond donor at this point. The protonation coupled to the reduction of NCO^- supports the presence of a carbamoyl ligand. Inhibition by NCO^-, like the activation of CO_2, thus seems to rely on $2e^-$ reduction after NCO^- binding. Further reaction of the bound carbamoyl ligand is likely hampered by the high activation barriers of 73–78 kcal mol^{-1}.[18]

True atomic resolution structures offer several advantages: 1) they allow a detailed analysis of the geometry of the bound substrate/inhibitor and 2) they reveal details of the metal coordination, including the metal–substrate interaction. Atomic resolution is especially helpful for understanding of CODHs, which are notoriously heterogeneous, with incompletely occupied metal centers in the active-site cluster, thus making the structural analysis of small-molecule ligands challenging.

The bond lengths and bent geometries found in the CO_2- and NCO^--bound states show that the same factors in CODH are responsible for the activation of CO_2 and mechanism-dependent inhibition by NCO^-: stable μ_2,η^2 coordination by Ni and Fe2 (Figure 4) combined with reductive activation formally by two electrons. The observation of the two-electron-reduced CO_2 bound to the cluster indicates that C–O bond cleavage is rate limiting in the crystal. This step likely involves protonation of the Fe-bound oxygen atom, the short C–O bond of which implies that the CO_2 ligand is not protonated in the structure.

The structures highlight the unusual properties of the Ni ion. While the observed nearly perfect square-planar coordination supports and extends our earlier findings (see Figure S3),[14] the atypical binding of NCO^-, as well as the very short Ni–C bonds with both ligands, indicate an unusual electronic structure for Ni, which likely originates from its integration into the Fe/S scaffold.

Both aspects, namely ligand geometry and Ni properties, indicate that "bifunctional catalysis" by a juxtaposed electrophilic Fe center and a nucleophilic Ni center is important but not sufficient to explain the reactivity of CODHs.[3c] The presented results emphasize the importance of a highly nucleophilic Ni center in the C_{red2} state, the electronic structure of which is optimized to reductively activate CO_2 and stabilize the two-electron-reduced intermediate through π backbonding. A major challenge for the future will be to mimic these properties in synthetic Ni complexes and harness the catalytic power of these complexes for efficient large-scale CO_2 conversion.

Keywords: biocatalysis · carbon dioxide · CO dehydrogenase · cyanate · reductive activation

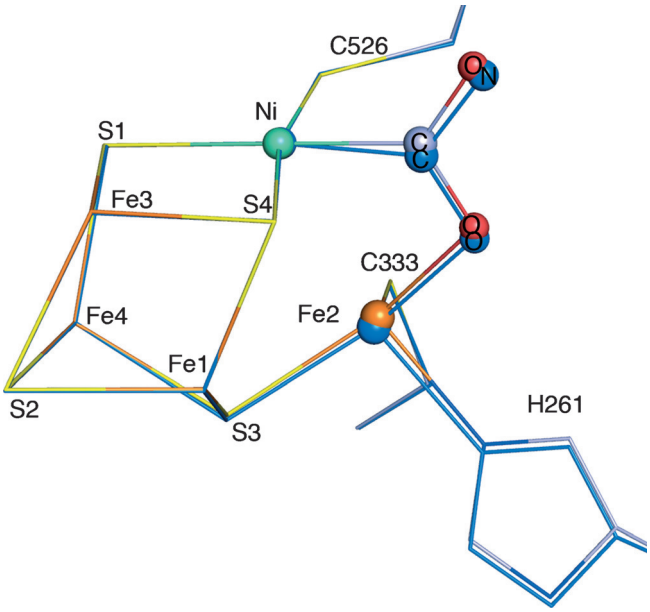

Figure 4. Superposition of CO_2 (element colors) and NCO^- bound to cluster C (marine blue). Coordinating cysteine residues for Fe1, Fe3, and Fe4 are not shown.

How to cite: *Angew. Chem. Int. Ed.* **2015**, *54*, 8560–8564
Angew. Chem. **2015**, *127*, 8680–8684

[1] a) K. S. Lackner, *Science* **2003**, *300*, 1677–1678; b) M. Rakowski DuBois, D. L. DuBois, *Acc. Chem. Res.* **2009**, *42*, 1974–1982; c) R. Schlögl, *Angew. Chem. Int. Ed.* **2011**, *50*, 6424–6426; *Angew. Chem.* **2011**, *123*, 6550–6553.
[2] E. E. Benson, C. P. Kubiak, A. J. Sathrum, J. M. Smieja, *Chem. Soc. Rev.* **2009**, *38*, 89–99.
[3] a) H. J. Freund, M. W. Roberts, *Surf. Sci. Rep.* **1996**, *25*, 225–273; b) Y. Toda, H. Hirayama, N. Kuganathan, A. Torrisi, P. V. Sushko, H. Hosono, *Nat. Commun.* **2013**, *4*, 2378; c) A. M. Appel, et al., *Chem. Rev.* **2013**, *113*, 6621–6658; d) Q. Lu, J. Rosen, Y. Zhou, G. S. Hutchings, Y. C. Kimmel, J. G. G. Chen, F. Jiao, *Nat. Commun.* **2014**, *5*, 0; e) J. L. Qiao, Y. Y. Liu, F. Hong, J. J. Zhang, *Chem. Soc. Rev.* **2014**, *43*, 631–675.
[4] a) M. Can, F. A. Armstrong, S. W. Ragsdale, *Chem. Rev.* **2014**, *114*, 4149–4174; b) J. H. Jeoung, J. Fesseler, S. Goetzl, H. Dobbek in *Metal Ions in Life Sciences*, *Vol. 14* (Eds.: P. M. H. Kroneck, M. E. Sosa Torres), Springer, Heidelberg, **2014**, pp. 37–69.
[5] a) S. A. Ensign, *Biochemistry* **1995**, *34*, 5372–5381; b) V. Svetlitchnyi, C. Peschel, G. Acker, O. Meyer, *J. Bacteriol.* **2001**, *183*, 5134–5144.
[6] J. H. Jeoung, H. Dobbek, *Science* **2007**, *318*, 1461–1464.
[7] a) D. A. Grahame, E. Demoll, *Biochemistry* **1995**, *34*, 4617–4624; b) P. A. Lindahl, E. Munck, S. W. Ragsdale, *J. Biol. Chem.* **1990**, *265*, 3873–3879; c) P. A. Lindahl, S. W. Ragsdale, E. Munck, *J. Biol. Chem.* **1990**, *265*, 3880–3888.
[8] a) J. Seravalli, M. Kumar, W. P. Lu, S. W. Ragsdale, *Biochemistry* **1995**, *34*, 7879–7888; b) V. C. Wang, M. Can, E. Pierce, S. W. Ragsdale, F. A. Armstrong, *J. Am. Chem. Soc.* **2013**, *135*, 2198–2206.
[9] a) T. Gruene, H. W. Hahn, A. V. Luebben, F. Meilleur, G. M. Sheldrick, *J. Appl. Crystallogr.* **2014**, *47*, 462–466; b) G. M. Sheldrick, T. R. Schneider, *Methods Enzymol.* **1997**, *277*, 319–343.

[10] W. M. Haynes, *CRC Handbook of Chemistry and Physics, Vol. 91*, CRC, Boca Raton, FL, **2010**.
[11] D. H. Gibson, *Chem. Rev.* **1996**, *96*, 2063 – 2095.
[12] M. Aresta in *Activation of Small Molecules*, (Ed.: W. B. Tolman), Wiley-VCH, Weinheim, **2006**, pp. 1 – 41.
[13] J. W. Rabalais, J. M. McDonald, V. Scherr, S. P. McGlynn, *Chem. Rev.* **1971**, *71*, 73 – 108.
[14] a) F. Holtzberg, B. Post, I. Fankuchen, *Acta Crystallogr.* **1953**, *6*, 127 – 130; b) C. Yoo, J. Kim, Y. Lee, *Organometallics* **2013**, *32*, 7195 – 7203; c) Y. L. Yang, J. D. Chen, Y. C. Lin, M. C. Cheng, Y. Wang, *J. Organomet. Chem.* **1994**, *467*, C6 – C8; d) D. H. Gibson, M. Ye, B. A. Sleadd, J. M. Mehta, O. P. Mbadike, J. F. Richardson, M. S. Mashuta, *Organometallics* **1995**, *14*, 1242 – 1255.
[15] E. J. Kim, J. Feng, M. R. Bramlett, P. A. Lindahl, *Biochemistry* **2004**, *43*, 5728 – 5734.
[16] a) I. Ben Moussa, M. S. Belkhiria, S. Najmudin, C. Bonifacio, H. Nasri, *Acta Crystallogr. Sect. E* **2011**, *67*, m903 – m904; b) A. B. Caballero, M. Quiros, A. Rodriguez-Dieguez, J. M. Salas, *Acta Crystallogr. Sect. E* **2011**, *67*, m345; c) M. Wriedt, I. Jess, C. Nather, *Acta Crystallogr. Sect. E* **2009**, *65*, m431; d) D. P. Zhang, *Acta Crystallogr. Sect. E* **2010**, *66*, m1656.
[17] a) D. M. Duggan, D. N. Hendrick, *Inorg. Chem.* **1974**, *13*, 2056 – 2062; b) Z. Mahendrasinh, S. Ankita, S. B. Kumar, A. Escuer, E. Suresh, *Inorg. Chim. Acta* **2011**, *375*, 333 – 337.
[18] V. S. Nguyen, H. L. Abbott, M. M. Dawley, T. M. Orlando, J. Leszczynski, T. N. Minh, *J. Phys. Chem. A* **2011**, *115*, 841 – 851.

Received: February 24, 2015
Published online: April 29, 2015

